J Stat Phys (2017) 167:656–682
DOI 10.1007/s10955-016-1559-z

Arrested Bubble Rise in a Narrow Tube

Catherine Lamstaes[1] · **Jens Eggers**[1]

Received: 27 February 2016 / Accepted: 3 June 2016 / Published online: 13 June 2016

Abstract If a long air bubble is placed inside a vertical tube closed at the top it can rise by displacing the fluid above it. However, Bretherton found that if the tube radius, R, is smaller than a critical value $R_c = 0.918\ \ell_c$, where $\ell_c = \sqrt{\gamma/\rho g}$ is the capillary length, there is no solution corresponding to steady rise. Experimentally, the bubble rise appears to have stopped altogether. Here we explain this observation by studying the unsteady bubble motion for $R < R_c$. We find that the minimum spacing between the bubble and the tube goes to zero in limit of large t like $t^{-4/5}$, leading to a rapid slow-down of the bubble's mean speed $U \propto t^{-2}$. As a result, the total bubble rise in infinite time remains very small, giving the appearance of arrested motion.

Keywords Singularities · Thin film flow · Lubrication theory · Surface tension

1 Introduction

A very common and useful observation, for example in the biological sciences, is that the flow of liquid out of a narrow capillary can be arrested by sealing off the top or bottom (for example using a finger). This is illustrated in the sequence on the right of Fig. 1: a capillary of inner radius $R = 1.9$ mm is closed off at the bottom. As a result, a column of water remains suspended above the air bubble at the bottom, without any apparent motion, even over long periods of time.

This observation appears to contain a paradox, since the buoyancy of the bubble exerts a force on the liquid, which is compensated by an opposing force from the liquid. A viscous liquid, however, cannot sustain a permanent tangential stress; a viscous force can only result if there is at least some motion. In all cases studied here, we assume the inner wall of the tube

✉ Jens Eggers
jens.eggers@bris.ac.uk

[1] School of Mathematics, University of Bristol, University Walk, Bristol BS8 1TW, UK

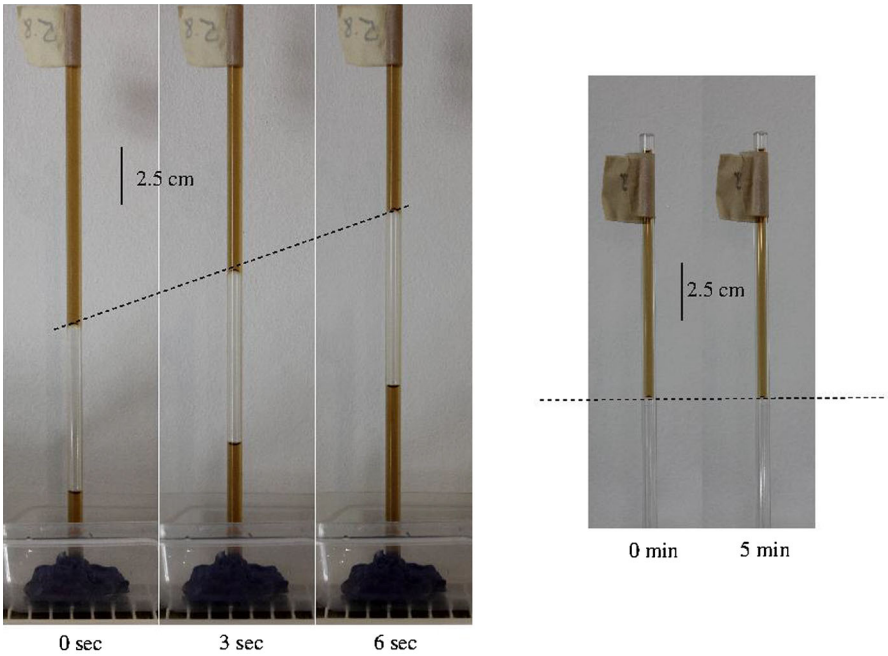

Fig. 1 A home experiment illustrating the motion of long bubbles in tubes filled with water (using coffee as a colorant), closed off at the end. Based on the surface tension of water, $R_c \approx 2.5$ mm. *On the left*, a bubble rises steadily in a tube with inner radius $R = 2.9$ mm. On the *right*, no motion is detectable evenover a long period in a tube with $R = 1.9$ mm

to have been prewetted, or the fluid to wet the walls perfectly, so all of the solid is covered by at least a thin film of liquid. As a result, there are no contact lines to be considered.

The setup shown on the left of Fig. 1 differs from that on the right only by the radius of tube, which at $R = 2.9$ mm is slightly wider. But now buoyancy drives a viscous flow: as an air bubble rises at a constant rate, fluid escapes from above the bubble, passes through a thin film surrounding the bubble, and eventually adds to the fluid below the bubble. The present paper is devoted to resolving the paradox of the stuck bubble, and to explain the difference between the two experiments shown in Fig. 1.

In his classical paper [1], Bretherton considers the theory of the slow motion of long bubbles (much longer than the radius of the tube) in circular tubes. The tube is filled with liquid of dynamic viscosity η and density ρ, having interfacial tension γ between the bubble and liquid. In the first part of the paper, gravity is not considered, and bubbles are set in motion by pushing liquid through the tube. The second part of the paper, which appears to be much less well known, addresses the problem shown in Fig. 1: tubes are placed vertically and are sealed at the bottom end, so that gravity is the driving force. The theory is developed for narrow tubes, whose radii are in the order of the capillary length and below. Therefore, if U is the speed of the bubble, the Reynolds number $\mathrm{Re} = \rho \mathrm{UR}/\eta$ is considered small, and inertial effects do not play any role. Looking for traveling wave solutions describing the rise of a bubble at constant speed U (the bubble is always considered to be far from the ends of the tube), Bretherton finds a solution only if the radius R of the tube is larger than a critical radius $R_c = 0.918\ \ell_c$, where $\ell_c = \sqrt{\gamma/\rho g}$ is the capillary length, and g is the acceleration of gravity. As the critical radius is approached, the speed of the bubble goes to zero.

In [1], no theoretical argument is given as to what might happen for $R < R_c$, but experimental evidence is cited that a smaller bubble does not move. There is the possibility that other traveling wave solutions exist for $R < R_c$, of a form not anticipated in the original analysis. Apart from that, the only other possibility is that the real solution is unsteady in some way. Since the bubble can move only by fluid moving past it, an apparent cessation of motion implies that the flux through the film goes to zero. We will see that this is because the film pinches off as its thickness approaches zero locally, so owing to the no-slip boundary condition at the wall less and less fluid is able to pass through. This implies that the bubble motion is slowed down, and if this slowing is sufficiently rapid, the bubble will move only a *finite* distance in infinite time, and its motion appears arrested.

Almost exactly 25 years ago, Leo Kadanoff at the University of Chicago initiated a research program, which brought together Mathematicians, Physicists, and Computer Scientists to look at singularities of nonlinear partial differential equations. A lot of effort had been devoted to finding singular solutions to the Euler equation in three dimensions, a problem thought to be relevant to fluid turbulence, but there had been little progress. Leo's idea was to take much simpler one-dimensional equations, such as the equation describing thin film flow, and to develop tools, both analytical and numerical, to gradually chip away at singular problems. A diverse group of people from senior professors (e.g. Peter Constantin), to first-year graduate students (e.g. Michael Brenner), met each week at "The Barn" in Ryerson Physical Laboratory to exchange ideas. The result was a first series of papers on thin film equations [2–5], and the inspiration for many to look at PDE's from a new angle [6], using scale invariance as the guiding principle.

Here we draw on the insights from this early period to address the pinch problem that must be taking place in a vertical tube for $R < R_c$. In [4] it has been conjectured that for a thin film flowing over a solid substrate, the thickness can never reach zero in finite time. Hence we anticipate that the thickness goes to zero in infinite time, forming an *infinite time singularity*. We will see that gravity comes into our problem in an essential way, leading to a novel set of scaling exponents, different from that found in related problems, such as the drainage of the thin film of liquid between two drops approaching one another [7]. We will make extensive use of Leo Kadanoff's insight that singularities are governed by similarity solutions [8], whose typical scales are described by power laws.

In the next section, we will revisit Bretherton's theory of steady bubble motion in a vertical tube, valid for $R > R_c$. We then describe numerical simulations of a model equation which captures the leading-order asymptotics of the bubble motion. This allows us to contrast the case $R > R_c$, for which we converge toward a steady solution, with the unsteady motion in the case $R < R_c$, during which the film thickness goes to zero in infinite time. In the fourth section, we develop an asymptotic theory of the pinch-off observed for $R < R_c$. This solution is divided into three asymptotic regions: the central pinch-off region, where the minimum film thickness lies, is matched to a static outer region at the top of the bubble. The nature of this outer region decides whether pinch-off is observed or not. Below the pinch point, the pinch region matches onto a thin film region, governed by a novel similarity solution to the thin film equations, where capillary, gravitational, and time-dependent terms all come in at the same order. We conclude this section with a summary of observable results from our theory. In the final discussion we contrast our solution with those found previously, and present an outlook on future lines of research.

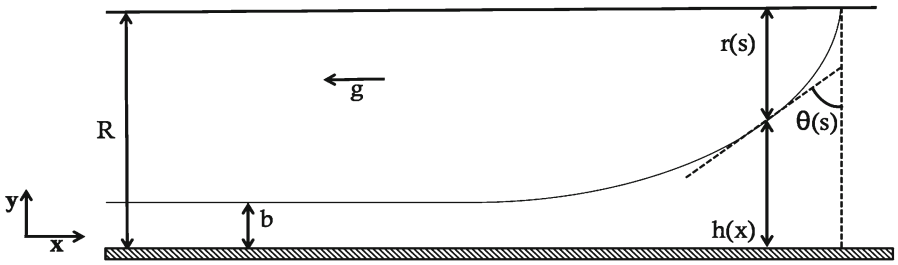

Fig. 2 Sketch of a bubble in a vertical tube. The angle θ is measured anti-clockwise from the y-direction to the tangent of the interface. The distance s is the arc-length of the interface measured from the line of symmetry

2 Bretherton's Theory of Steady Motion

We begin by recalling Bretherton's previous theory [1] for the dynamics of a bubble in a vertical tube, which assumes that the bubble rises at a constant speed U. We aim to formulate his approach more systematically using the method of matched asymptotic expansions [9], although our final result will turn out to be equivalent to Bretherton's. We consider both the axisymmetric case of a cylindrical tube of radius R (see Fig. 2), as well its two-dimensional analogue of two vertical plates a distance of $2R$ apart for which some of the calculations can be performed analytically. The coordinate x denotes the vertical distance against the direction of gravity, and $h(x)$ is the (radial) thickness of the film between the bubble and the walls (of the tube).

We aim to describe the transition between moving and arrested bubbles, near which the bubble speed U goes to zero, so we are in a regime where the capillary number $\mathrm{Ca} = \eta \mathrm{U}/\gamma$ is small. As a result, viscous deformations of the interface are small, and the solution can be split into two asymptotic regions, similar to the structure of the celebrated Landau–Levich problem [10]. The first (outer) region describes the top of the bubble, which is controlled by a balance of surface tension and gravity, while viscous forces are negligible on the scale of the tube radius R. The second (inner) region describes the thin film between the bubble and the tube wall. In this region, viscous, surface tension, and gravitational forces are balanced. Owing to $\mathrm{Ca} \ll 1$, lubrication theory applies [11]. To find a complete solution in the limit $\mathrm{Ca} \ll 1$, the two regions will be combined using a matched asymptotic expansion [9].

2.1 Static Cap Solution

Since surface tension and gravity are of the same order, it is convenient to write all lengths in units of the capillary length ℓ_c. With this convention, R^2 is commonly called a Bond number, which is of order one for our problem. Balancing capillary pressure and hydrostatic pressure in the fluid, the static surface shape is described by $p = 0 = -\kappa + x$, where κ is (twice) the mean curvature of the interface. Thus if s is the arclength of the interface and θ the tangent angle with respect to the vertical, we have

$$\kappa^{(2D)} = \frac{d\theta}{ds}, \qquad \kappa^{(3D)} = \frac{d\theta}{ds} + \frac{\sin\theta}{r} \tag{1}$$

in two and three dimensions, respectively. To find the outer solution, we have to solve the equations

$$x = \kappa, \qquad \frac{dx}{ds} = -\sin\theta, \qquad \frac{dr}{ds} = \cos\theta. \tag{2}$$

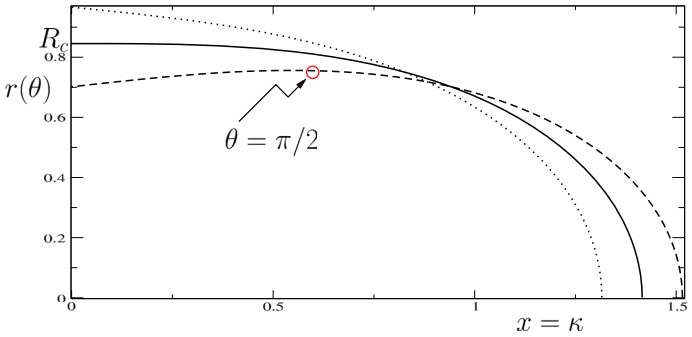

Fig. 3 A plot of (3), (4) in the region of positive curvature, from $\theta = 0$ (tip) to $\theta = \theta_I$ (inflection point), for $\theta_I = \pi/2$ (*solid line*), $\theta_I > \pi/2$ (*dashed line*) and $\theta_I < \pi/2$ (*dotted line*). Only curves with $\theta_I >= \pi/2$ have a maximum radius, where $\theta = \pi/2$; the maximum radius for $\theta_I = \pi/2$ is R_c

For simplicity, we will focus on the two-dimensional case, for which the solution can be found analytically. Namely, in two dimensions the equation for the static profile becomes $\theta_{ss} = -\sin\theta$, with initial condition $\theta(0) = 0$ at the tip of the bubble. Integrating this equation gives

$$x(\theta) = \kappa = \frac{d\theta}{ds} = \pm\sqrt{2\,(\cos\theta - \cos\theta_I)}, \tag{3}$$

where θ_I is the angle at the inflection point $x = \kappa = 0$. We see that the angle is always in the range $0 \le \theta \le \theta_I$, while the + and − signs in (3) describe the regions of positive and negative curvature, respectively. We are interested in the region closest to the tip only, for which $x > 0$ (+ sign in (3)). There the distance from the center of the tube to the interface is

$$r(\theta) = \frac{1}{\sqrt{2}}\int_0^\theta \frac{\cos\psi}{\sqrt{\cos\psi - \cos\theta_I}}d\psi = -\mathrm{F}\left(\frac{2\sin\theta/2}{x(\theta)}, \frac{x(\theta)}{2}\right) + 2\mathrm{E}\left(\frac{2\sin\theta/2}{x(\theta)}, \frac{x(\theta)}{2}\right), \tag{4}$$

where

$$\mathrm{F(x,k)} = \int_0^{\mathrm{x}} \frac{1}{\sqrt{1-\mathrm{k}^2\mathrm{t}^2}\sqrt{1-\mathrm{t}^2}}\mathrm{dt}, \qquad \mathrm{E(x,k)} = \int_0^{\mathrm{x}} \frac{\sqrt{1-\mathrm{k}^2\mathrm{t}^2}}{\sqrt{1-\mathrm{t}^2}}\mathrm{dt}$$

are the incomplete elliptic integrals of the first and second kinds, respectively. The radius $r(\theta)$ is related to the film thickness $h(x)$ by (cf. Fig. 2)

$$h(x) = R - r(\theta). \tag{5}$$

A plot of the outer solution (3), (4) is shown in Fig. 3 over the region where the curvature is positive. It follows from the last Eq. (2) that at a maximum of r, we must have $\theta = \pi/2$. Since $\theta < \theta_I$, only curves with $\theta_I > \pi/2$ have a maximum. We will see below that in order to match to the inner solution, the slope must be positive in the region of positive curvature, which is true only if $\theta_I < \pi/2$. The critical case is $\theta_I = \pi/2$, for which the radius at the inflection point is

$$R_c = \frac{1}{\sqrt{2}}\int_0^{\pi/2}\sqrt{\cos\psi}\,d\psi = \frac{\Gamma^2(3/4)}{\sqrt{\pi}} = 0.8472\ldots, \tag{6}$$

where Γ denotes the Gamma function. This is the critical radius below which matching is no longer possible, so no traveling wave solutions exist. In the axisymmetric case, a numerical approximation yields $R_c^{(3D)} = 0.918$ [1].

2.2 Film Solution

We now describe the thin film along the sides of the bubble, where the slope is small, and we can use the lubrication equations for the flow of a thin film of viscous liquid over a solid wall [8]. Since the film thickness is much smaller than the tube radius R, we can neglect the tube's curvature (in the three-dimensional case), making the problem effectively two-dimensional. In the lubrication approximation, the viscous flow is driven by a pressure gradient, which has contributions from the capillary and the hydrostatic pressure. Thus as the unit of time, we choose $\tau = \eta \ell_c/\gamma$, so the speed U of the bubble is the capillary number. Apart from the final subsection where we present results in dimensional form, everything will from now on be written in units of ℓ_c and τ. The volume flux, in a stationary frame of reference, becomes

$$Q = \frac{h^3}{3} p_x = \frac{h^3}{3}(h_{xxx} - 1). \tag{7}$$

The term h_{xxx} comes from the gradient of the Laplace pressure, in the limit that the interface is nearly parallel to the wall, while the second term is the gradient of the hydrostatic pressure.

In a situation in which the bubble rises at a constant speed U and the tube is closed, the flux past the bubble is set by the amount of fluid displaced above the bubble. In a frame of reference in which the tip of the bubble is stationary, the top comes toward the bubble at a speed U. Thus the volume displaced per unit time is $\pi R^2 U$ in three dimensions, and $2RU$ per unit width in two dimensions. This means that in the frame of reference of the bubble, the flux per unit width Q_b through the film is

$$Q_b^{(2D)} = -UR, \qquad Q_b^{(3D)} = -UR/2 \tag{8}$$

in two and three dimensions, respectively. Transforming to a stationary frame of reference, the flux becomes $Q = Q_b + hU$. However, since $h \ll R$, this correction is subdominant relative to (8), and we can think of the profile $h(x)$ as being time-independent, represented in a co-moving coordinate system, as indicated in Fig. 2. Thus using (7), the thin film equation for the gap h becomes

$$h_{xxx} = 1 - \frac{b^3}{h^3}, \tag{9}$$

where $b^3 = 3RU$ in two dimensions, and $b^3 = 3RU/2$ in three dimensions. The quantity b can be interpreted as the constant film thickness far away from the tip, cf. Fig. 2.

Equation (9) describes the *inner solution* of our problem, governed by the length scale b. Looking for a similarity solution of the form

$$h(x) = b\eta(\xi), \quad \xi = x/b^{1/3}, \tag{10}$$

(9) becomes

$$\eta_{\xi\xi\xi} = 1 - \eta^{-3}. \tag{11}$$

In this equation, surface tension forces (the term on the left) are balanced by gravity (first term on the right) and viscous forces (second term on the right).

2.3 Matching

We have to match the inner solution, described by (11), to the static outer solution (4), valid near the end of the bubble. Since $b \ll R$, this amounts to taking the limit of large η in the

inner solution. But for large η, (11) asymptotes to $\eta_{\xi\xi\xi} \simeq 1$, so the general solution of (11) in this limit is

$$\eta = \frac{\xi^3}{6} + a_2\xi^2 + a_1\xi + a_0. \tag{12}$$

Since (11) is autonomous, we can always shift the origin such that the coefficient a_2 is made to vanish, giving zero curvature at ξ_0:

$$\eta = \frac{(\xi - \xi_0)^3}{6} + a_1(\xi - \xi_0) + a_0, \qquad \xi \to \infty. \tag{13}$$

The coefficients a_1 and a_0 are now determined uniquely, and have to be found by integrating (11) from the region of constant film thickness $\eta = 1$.

To that end, we consider a small perturbation from a film of constant thickness

$$\eta = 1 + \epsilon e^{\lambda\xi}. \tag{14}$$

Inserting (14) into (11) and linearizing, we find $\lambda^3 = 3$. We are interested in roots λ with positive real part only, since negative roots do not satisfy the boundary condition $\eta = 1$ for $\xi \to -\infty$. Thus, the only relevant perturbation is of the form

$$\eta = 1 + \epsilon e^{3^{1/3}\xi}. \tag{15}$$

The value of ϵ can be changed by shifting the ξ variable: we can put $\epsilon = 1$, but choose the initial value of ξ to be a large negative number, so the linear approximation is valid. Using (15) to find the initial conditions and integrating (11) forward toward $\xi = \infty$, one finds the coefficients of the expansion (12). Choosing ξ_0 such that the quadratic coefficient cancels, one finds the *universal* constants $a_1 = 0.572$ and $a_0 = 1.097$. These values agree with those found by Bretherton. In terms of the outer variables, the outer limit of the inner solution is

$$h = \frac{x^3}{6} + a_1 b^{2/3} x + a_0 b. \tag{16}$$

A technical problem associated with the matching to the outer solution is that both solutions can be shifted by an arbitrary distance in the x-direction. To fix this shift, Bretherton chose to expand both solutions about the point of zero curvature. What is slightly confusing about this choice is that the full solution of (11) actually has positive curvature everywhere, and only its outer expansion (16) has vanishing curvature. To clarify this issue, we take as the point around which to match the inner and outer solutions as the one satisfying $h(x_m) = h_m$, where the height h_m is chosen to lie between the length scales of the inner and outer solutions: $b \ll h_m \ll R$. By this choice, we ensure that $\kappa > 0$, see Fig. 4. In the limit $b \to 0$, the asymptotic conditions on h_m are satisfied by the choice $h_m = b^\alpha$, where $\alpha \in (0, 1)$. We will verify that the result does not depend on on the particular choice of α.

Denoting the film height in the inner and outer solutions by $h_i(x)$ and $h_o(x)$, respectively, we require the matching conditions

$$h_i(x_m) = h_o(x_m), \qquad h_i'(x_m) = h_o'(x_m), \qquad h_i''(x_m) = h_o''(x_m), \tag{17}$$

where for the inner solution we take the outer limit (16). In (17) and in the following, primes denote the derivative. According to (2) and (16), both inner and outer solutions satisfy $h'''(x_m) = 1$, which means that to leading order gravity and surface tension are balanced. The matching between the inner and outer solutions is illustrated in Fig. 4.

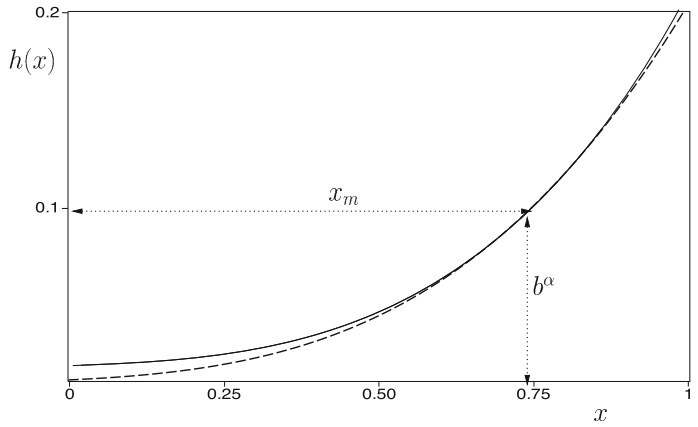

Fig. 4 Matching of the inner solution (*dashed line*) and outer solution (*solid line*) of $h(x)$ for $b = 10^{-2}$. The two curves are matched about the point $h_m = b^{1/2} = 0.1$ ($\alpha = 1/2$). The outer solution has been chosen such that the two curves are identical at h_m. In this case one finds the outer solution to be a tube of radius $R = 0.879$

We now evaluate each term in (17) in the limit $b \to 0$. It follows from (16) that to leading order $b^\alpha \approx x_m^3/6$, and using successive approximations we find

$$x_m \approx 6^{1/3} b^{\alpha/3} - 2a_1 6^{-1/3} b^{(2-\alpha)/3} - 2a_0 6^{-2/3} b^{(3-2\alpha)/3}, \tag{18}$$

so that

$$h_i'(x_m) \approx 6^{2/3} b^{2\alpha/3}/2 - a_1 b^{2/3} - 2a_0 6^{-1/3} b^{(3-\alpha)/3}, \quad h_i''(x_m) \approx x_m. \tag{19}$$

Since h' goes to zero, we can approximate

$$h_o'' \approx \kappa = \sqrt{2(\cos\theta_m - \cos\theta_I)}, \qquad h_o' = -r_x(\theta_m) = \cot\theta_m \approx \cos\theta_m,$$

so that using the last two of the matching conditions (17) we obtain

$$\cos\theta_m \approx h_i'(x_m), \qquad \cos\theta_I \approx h_i'(x_m) - h_i''^2(x_m)/2 = a_1 b^{2/3}. \tag{20}$$

The first matching condition (17) becomes

$$R - b^\alpha = r(\theta_m) = r(\theta_I) + \frac{1}{\sqrt{2}} \int_{\theta_I}^{\theta_m} \frac{\cos\psi}{\sqrt{\cos\psi - \cos\theta_I}} d\psi \equiv r(\theta_I) + \epsilon(\theta_m, \theta_I), \tag{21}$$

which we have to evaluate in the limit $\theta_m \to \pi/2$ and $\theta_I \to \pi/2$, since both right hand sides of (20) go to zero.

Beginning with the first integral of (21), we find

$$r(\theta_I) \approx \frac{1}{\sqrt{2}} \int_0^{\pi/2} \frac{\cos\psi}{\sqrt{\cos\psi - \cos\theta_I}} d\psi = \frac{1}{\sqrt{2}} \int_0^{\pi/2} \sqrt{\cos\psi}\, d\psi +$$
$$\frac{a_1 b^{2/3}}{2} \frac{1}{\sqrt{2}} \int_0^{\pi/2} \frac{1}{\sqrt{\cos\psi}} d\psi + O(b^{4/3}) = R_c + K\left(1/\sqrt{2}\right) \frac{a_1 b^{2/3}}{2} + O(b^{4/3}), \tag{22}$$

where $K(1/\sqrt{2}) = \pi^{3/2}/(2\Gamma^2(3/4))$ denotes the complete elliptic function of the first kind. As for $\epsilon(\theta_m, \theta_I)$ in (21), we use (20) to find:

$$\epsilon(\theta_m, \theta_I) \approx \frac{1}{\sqrt{2}} - \int_{a_1 b^{2/3}}^{h_i'(x_m)} \frac{\Delta}{\sqrt{\Delta - \Delta_I}} d\Delta \approx -b^\alpha + a_0 b. \tag{23}$$

Combining (21), (22) and (23) we finally obtain

$$R - R_c = 0.5302\, b^{2/3} + 1.097\, b, \quad b^3 = 3RU, \quad R_c = 0.8472. \quad \text{(2D)} \tag{24}$$

The value of the exponent α, used to perform the matching, does not enter, as should be the case. The relation (24) is the two-dimensional version of the original result given in [1], valid for circular tubes of radius R, which can be written in the same form:

$$R - R_c = 0.582\, b^{2/3} + 1.01\, b, \quad b^3 = 3RU/2, \quad R_c = 0.918. \quad \text{(3D)} \tag{25}$$

If $R > R_c$, the bubble moves at a constant speed U, and the thickness of the film in the tail of the bubble is b, both given by (24) or (25). As the critical radius R_c is approached, this speed goes to zero. For $R < R_c$, the inner and outer solutions can no longer be matched, and there is no solution corresponding to a bubble rising at constant speed. The rest of our paper will be devoted to calculating the unsteady motion that takes place in that case.

3 Numerical Description

Before we explain in detail the similarity theory of pinch-off for the case $R < R_c$, we introduce a numerical description of the bubble which is valid close to the critical radius R_c, so that the bubble is moving very slowly. This will give is some insight into the bubble's behavior on both sides of the critical radius. We will use the numerical results to compare the dynamics of the bubble with that predicted by the similarity theory.

Following previous authors [12,13], we use a generalized lubrication theory, in which we replace the flat-film approximation to the curvature, h_{xx}, by the full curvature at the interface,

$$\kappa = \frac{h_{xx}}{\left(1 + h_x^2\right)^{3/2}}. \tag{26}$$

Then the two-dimensional volume flux (7) becomes

$$Q = h^3(\kappa_x - 1)/3, \tag{27}$$

and the equation of motion is

$$\frac{\partial h}{\partial t} + \frac{1}{3}[h^3(\kappa_x - 1)]_x = 0. \tag{28}$$

In the thin film region, $h_x \ll 1$, this equation coincides with the conventional lubrication equation. On the other hand, near the end of the bubble, controlled by a balance between capillarity and gravity, (28) reduces to the static balance described by (2). For $R > R_c$, time-independent solutions of (28) correspond to the steady solution described in the previous section.

We solve (28) using an adaptation of the finite-difference code used in [4,14]. At each time step, the left-hand side of (28) is discretized using a centered differences scheme. It is then advanced in time using a second-order accurate implicit scheme. An adaptive grid is used to obtain high resolution near the pinch point where h goes to zero [8]. To simulate

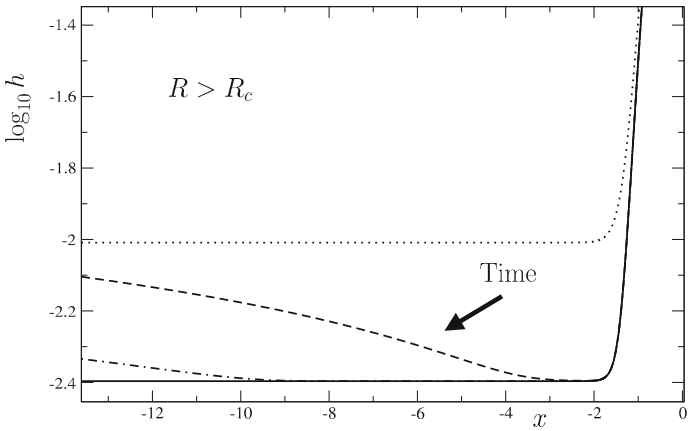

Fig. 5 Plot of the film height $h(x,t)$ (2D model) for $R = 0.865$ at time $t = 0$ (*dotted*), $\log_{10} t = 1.61$ (*dashed*), 2.36 (*dash-dotted*), and 3.11 (*solid lines*). The film quickly approaches a film of minimum height $\log_{10}(b) \approx -2.40$. The theoretical value according to (24) is $\log_{10}(b) \approx -2.397$. The initial film profile is a rescaling of the profile of a traveling wave solution of a bubble traveling in a tube of radius $R = 0.88 > R_c$, scaled down by a factor of $a = 0.98$

large bubbles, we choose some large domain $x \in [-L, 0]$, where L is up to 10^9, using an expanding grid. For $x = 0$, h is held fixed at $h = R$ with infinite gradient ($h_x \to \infty$), at $x = -L$, boundary conditions are $h = b_{in}$ and $h_x = 0$.

Initial conditions are generated using the steady-state solutions described in Sect. 2, rescaling them in order to generate solutions with either $R > R_c$ or $R < R_c$; as a result, they are no longer steady-state solutions of (28). Figure 5 shows the case $R = 0.865 > R_c$, but with an initial film thickness b_{in} greater than the steady-state value $b = 4.01 \times 10^{-3}$ given by (24). In time, a wave travels from the tip of the bubble toward the tail. After the wave has passed, the film thickness has reached a stationary value, which is very close to the theoretical prediction. This confirms that the steady state of Sect. 2 is indeed a globally attracting solution, in agreement with [1].

If on the other hand $R < R_c$, the behavior is very different, as seen in Fig. 6. Instead of converging to a stationary solution, in the long-time limit the profile pinches down in a localized fashion. In order to study the pinch-off down to very small minimum heights, we have to follow the solution for very long times. To that end we adopt a slightly different procedure to that in the case $R > R_c$. We know from the theory to be reported below that far downstream from the bubble tip, and in the limit of long times, the profile is asymptotically:

$$h(x,t) = t^{-1/2}\sqrt{x_0 - x}, \tag{29}$$

where x_0 is the pinch point. Thus in an initial period, we simulate (28), with the boundary condition of constant film thickness at $x = -L$, until h has converged to a profile of the form (29) over an x-region of order L. However, we make sure that the initial profile is still unperturbed near the left-hand end of the interval. Once the the solution is well converged, we cut the original interval to an interval of size $O(1)$, on whose left-hand boundary we impose (29) as a time-dependent boundary condition, where x_0 is determined as a fit paramter to the numerical profile. This permits us to simulate (28) for sufficiently long periods so as to reach a minimum height of $h_{min} \approx 10^{-11}$, beyond which rounding errors become significant.

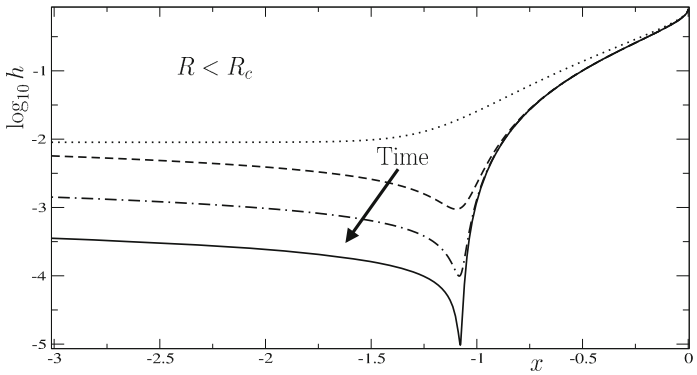

Fig. 6 Plot of the film height $h(x, t)$ (2D model) for R = 0.794 at time $t = 0$ (*dotted line*), $\log_{10}(t) = 3.02$ (*dashed line*), $\log_{10} t = 4.50$ (*dash-dotted line*) and $\log_{10} t = 7.02$ (*solid line*). The initial film profile is obtained in the same way as that of Fig. 5, but scaled down by a factor of $a = 0.9$. In the limit $t \to \infty$, the profile pinches down at $x_0 \approx -1.076$

As is seen in Fig. 6, the profile becomes more and more localized around the pinch point x_0. As a result, the flux of liquid across the minimum goes to zero, and so does the speed of the bubble, which is constrained by volume conservation. In the following section, we will present a similarity theory of the infinite-time singularity associated with pinch-off, and compare to the results of numerical simulations.

4 Similarity Theory of Pinch-Off

We now study the unsteady bubble motion for $R < R_c$. For the bubble to get stuck in tubes with $R < R_c$, and as confirmed by Fig. 6, the minimum film height $h_{min}(t)$ has to tend to zero. As a result, the solution describing this pinch-off lacks a characteristic length scale, and we expect the local structure to be universal and self-similar [8].

Thus in the limit $t \to \infty$, we are looking for solutions of the form

$$h(x,t) = t^{\alpha} H(\xi), \quad \xi = \frac{x'}{t^{\beta}}, \quad x' = x - x_0 \tag{30}$$

where x_0 is the pinch point. We will assume that $\alpha < \beta$, so that $h_x \ll 1$. Then inserting (30) into (28) gives the similarity equation for the film:

$$\underbrace{t^{\alpha-1}(\alpha H - \xi\beta H_\xi)}_{T} + \underbrace{\frac{1}{3}t^{4\alpha-4\beta}\left(H^3 H_{\xi\xi\xi}\right)_\xi}_{Ca} - \underbrace{\frac{1}{3}t^{3\alpha-\beta}(H^3)_\xi}_{G} = 0. \tag{31}$$

Since different balances are possible, we have divided the similarity equation into 3 parts: terms coming from the time derivative are labeled 'T'; the term originating from surface tension has been labeled 'Ca', and that coming from gravity 'G'. We will show that the spatial structure of the film height $h(x, t)$ about the singularity can be described uniquely by three different dominant balances between 'T', 'Ca' and 'G', shown in Fig. 7. Each zone represents a different balance as follows:

In the Pinch-off Zone II, surface tension dominates terms 'G' and 'T' in (31), resulting in a Capillary-driven ('Ca') pinch-off. A similar central pinch region, controlled by surface

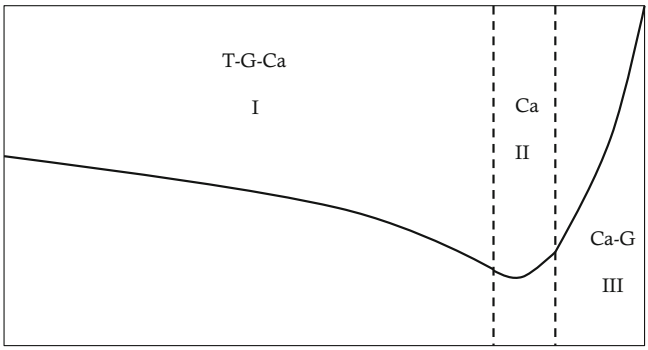

Fig. 7 Sketch of the three zones and corresponding balances of (31) that describes pinch-off of the film at the bubble's interface

tension alone, has been found in [4]. Zone III represents the time-independent static outer region given in (2). This corresponds to a 'Ca'–'G' balance in (31). Finally as one moves away toward the left of Zone II, contributions from 'T' and 'G' becomes increasingly important as the curvature of the profile decreases. This leads to a novel similarity solution which balances all three terms, 'T', 'Ca' and 'G' in (31). Below we describe the similarity solutions associated with each zone, characterized by a similarity profile $H(\xi)$ as well as scaling exponents α and β.

4.1 Zone II : The Pinch Region

For a 'Ca' dominated pinch-off, (31) reduces to

$$H^3 H_{\xi\xi\xi} = C, \tag{32}$$

where the constant of integration C is related to the surface-tension-driven current $j = h^3 h_{xxx}/3$ by $j = C/3t^{-4\alpha_2+3\beta_2}$. Equation (32) is known as the "current equation" [2], since it expresses the fact that the current is independent of position in the pinch region. The same similarity equation has also been considered in [7,15], as well as for a different power n ($H^n H_{\xi\xi\xi} = C$) in [2,4] and for $n = 2$ in [16]. As there is only a single term, the solution (32) does not fix either of the exponents $\alpha \equiv \alpha_2$ or $\beta \equiv \beta_2$ in its similarity representation (30). Instead, both exponents are found by matching to the two neighboring Zones I and III.

We anticipate that the typical scale of Zone II is much smaller than that of the neighboring zones, and so approaching Zone I corresponds to taking the limit $\xi \to -\infty$, while approaching Zone III corresponds to $\xi \to \infty$. This means we are interested in solutions to (32) which exist on the whole real axis, which we call global solutions. Two different asymptotic behaviors of (32) are possible as $\xi \to \pm\infty$ [4,7,16]. The generic case is quadratic growth, leading to an asymptotic expansion of the form:

$$H(\xi) = A\xi^2 + D\xi + E - \frac{C}{60A^3}\frac{1}{\xi^3} + O(\xi^{-4}), \quad |\xi| \to \infty. \tag{33}$$

All other coefficients are given in terms of A, D, E, corresponding to the full three-dimensional manifold of solutions. A singular limit of (33) is that $A \to 0$, in which case the asymptotic expansion becomes:

$$H(\xi) = B\xi + \frac{C}{2B^3}\log|\xi| + O(\xi^{-1}), \quad |\xi| \to \infty. \tag{34}$$

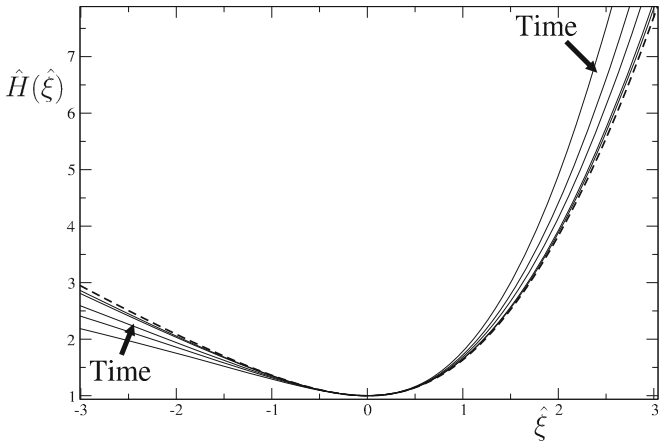

Fig. 8 The universal critical solution $\hat{H}(\hat{\xi})$ (*dashed line*), and numerical simulations of the full problem (*solid lines*) for R = 0.794, at $\log_{10}(t) = 7.18$, 8.47, 9.63, 10.88, and 12.11

The same asymptotic behavior can be generalized to any $n \geq 2$ [4,16]. To reach (34), a single parameter in the initial conditions to (32) has to be adjusted, leaving us with a two-dimensional manifold of solutions.

To find out how many distinct solutions to the current equation there are with H going to infinity like (34) and (33), note that (32) remains invariant under the transformation

$$H(\xi) = p\hat{H}(\hat{\xi}), \quad \hat{\xi} = \sqrt{\frac{q}{p}}\xi, \quad C = p^{5/2}q^{3/2}\hat{C}. \tag{35}$$

Since non-negative global solutions must have a minimum, there must be a point where $H_\xi = 0$, which owing to the translational invariance of (32) we can choose as the origin. Using the rescaling (35) we can ensure that at the origin values are normalized to

$$\hat{H}(0) = \hat{H}_{\hat{\xi}\hat{\xi}}(0) = 1, \quad \hat{H}_{\hat{\xi}} = 0, \tag{36}$$

and the rescaled equation becomes

$$\hat{H}^3\hat{H}_{\hat{\xi}\hat{\xi}\hat{\xi}\hat{\xi}} = \hat{C}. \tag{37}$$

Thus we expect a one-dimensional family of global solutions, parameterized by $\hat{C} \geq 0$, and with quadratic behavior (33) for $\xi \to \pm\infty$. We only need to consider non-negative $\hat{C}$, since the sign of $\hat{C}$ is flipped by a change in parity; for $\hat{C} = 0$, $\hat{H} = \xi^2/2 + 1$ is an exact solution. However, numerical integration of (37) with initial conditions (36) shows that such global solutions exist for $0 \leq \hat{C} < \hat{C}_c$ only, where

$$\hat{C}_c = 0.92842406\ldots, \tag{38}$$

in agreement with [7]. As the critical value $\hat{C}_c$ is approached from below, the quadratic coefficient A in the expansion for $\xi \to -\infty$ vanishes, and hence $\hat{C} = \hat{C}_c$ is the critical global solution which has linear behavior (34) for $\xi \to -\infty$, and quadratic behavior (33) for $\xi \to \infty$, see Fig. 8. No global solution is observed for $\hat{C} > \hat{C}_c$; instead, $\hat{H}_{\hat{\xi}\hat{\xi}}$ eventually becomes negative, leading to $\hat{H}(\xi) = 0$ at some finite value of ξ.

The critical solution is precisely the solution needed to solve our pinching problem. Namely, in Sect. 4.3 we will show that to match to an outer solution with time-independent positive curvature requires

$$h_{xx} = t^{\alpha_2 - 2\beta_2} H_{\xi\xi} = H_{\xi\xi} > 0.$$

Thus, we will obtain $\alpha_2 = 2\beta_2$ and we must have $H \approx A\xi^2$ as $\xi \to \infty$. On the other hand, in Sect. 4.2 we see that matching to a flat film on the left requires the profile to be linear, so we anticipate that $H \sim B\xi$ for $\xi \to -\infty$. For this critical solution, the quadratic and linear coefficients for $\xi \to \infty$ and $\xi \to -\infty$, respectively, are

$$\hat{A}_c = 0.84538\ldots, \quad \hat{B}_c = -1.10750\ldots. \tag{39}$$

In Fig. 8 this universal solution is shown as the dashed line. The sequence of solid lines is the simulation of (28) shown in Fig. 6, but rescaled according to (36). In the long-time limit, the local profile is seen to converge onto the global solution of (37). However, the region over which the full solution agrees with the similarity solution increases quite slowly, an issue to which we return in Sect. 4.4 below. Comparing to (34) and (33), one finds that

$$q = \frac{A}{\hat{A}}, \qquad p = \frac{\hat{A}}{A}\frac{B^2}{\hat{B}^2}, \tag{40}$$

so that $C = \hat{C}(B/\hat{B})^5 \hat{A}/A$. Below we calculate the constants A, B by matching the pinch region to Zones I and III, thus determining the scaling function $H(\xi)$ in the pinch region.

4.2 Zone I : Thin-Film Region

As we have argued before, we expect all three terms in (31) to balance in this region. Equating $\alpha_1 - 1 = 4\alpha_1 - 4\beta_1 = 3\alpha_1 - \beta_1$, one finds $\alpha_1 = -3/5$ and $\beta_1 = -1/5$:

$$h(x,t) = t^{-3/5} F(\eta), \quad \eta = \frac{x'}{t^{-1/5}}, \tag{41}$$

where F satisfies the fourth order ODE:

$$-\frac{3F}{5} + \frac{\eta F_\eta}{5} + \frac{1}{3}\left[F^3(F_{\eta\eta\eta} - 1)\right]_\eta = 0. \tag{42}$$

Toward the left, the limit $\eta \to -\infty$ describes the tail of the bubble. Toward the right, we match to Zone II, which is much smaller in size, corresponding to a constant value η_+.

In order to match to (34), and since the typical scale of the pinch region is small compared to that of the thin-film region, the solution of (42) must satisfy

$$F(\eta) \approx B\eta \tag{43}$$

as $\eta \to 0^-$. Equating (43) and (34) in the limit $x' \to 0^-$, we find

$$t^{-3/5} B\eta = t^{-2/5} Bx' = t^{\alpha_2} B\xi = t^{\alpha_2 - \beta_2} Bx',$$

and thus

$$\alpha_2 = \beta_2 - 2/5. \tag{44}$$

As shown in more detail in Appendix 1, the full asymptotic expansion of F in the limit $\eta \to 0^-$ is

$$F(\eta) = \sum_{j=1}^{\infty} \sum_{i=0}^{\max(j-2,1)} a_{ji} \eta^j (\log|\eta|)^i, \tag{45}$$

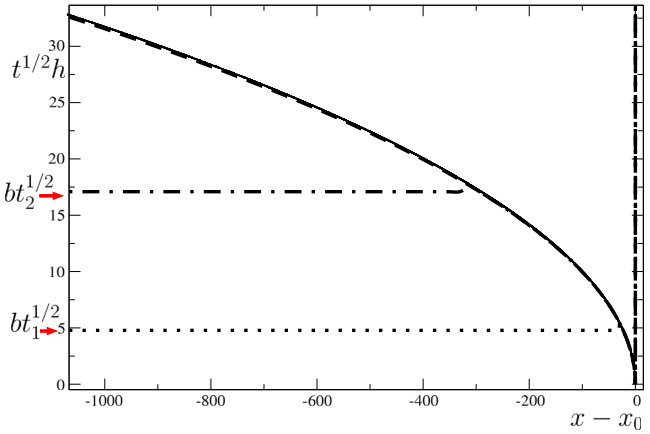

Fig. 9 Comparison of the asymptotic form (47) (*solid line*) with the simulation shown in Fig. 6, for $t_1 = 2.4 \times 10^5$ (*dotted line*), $t_2 = 2.9 \times 10^6$ (*dot-dashed line*), and $t_3 = 2.5 \times 10^7$ (*dashed line*). The initial film height is $b = 0.01$; the profiles at t_1 and t_2 are a constant film $h = b$ beyond the value of x' given by (48)

where the coefficients a_{ji} are given in terms of the two free parameters B and P. The first few coefficients are

$$a_{10} = B, \quad a_{11} = 0, \quad a_{20} = P - \frac{9}{20B^2}, \quad a_{21} = \frac{3}{10B^2},$$
$$a_{30} = -\frac{4P}{15B^3} + \frac{19}{75B^5} + \frac{1}{6}, \quad a_{31} = -\frac{2}{25B^5}, \quad \ldots. \tag{46}$$

To examine the behavior of F as $\eta \to -\infty$, we seek solutions of the form $F \approx a(-\eta)^m$, which yields two possible balances. First, for $m = 3$ one finds a balance $Ca \sim G >> T$. However, this would lead to an increasing curvature, which cannot be matched to a flat film. The other possibility is $m = 1/2$ and $a = 1$, which yields the balance $T \sim G >> Ca$ as $\eta \to -\infty$:

$$F(\eta) \approx \sqrt{-\eta}. \tag{47}$$

In outer variables, this yields the asymptotic form (29) of the tail of the bubble given earlier. The asymptotic form (47) is shown as the solid line in Fig. 9. Since the initial condition is such that $h = b = const$ toward the tail of the bubble, (47) breaks down when b is reached, leading to the condition

$$t^{-1/2}\sqrt{-x'} = b. \tag{48}$$

At a given time t, h is constant beyond the value of x' given by (48), as seen in the dotted and dot-dashed profiles in Fig. 9. The criterion (48) was used in the simulations described in Sect. 3: given the length L of the original computational interval, it determines the time $t = t_{thr}$ up to which the boundary condition of constant film thickness may be used.

As described in more detail in Appendix 2, the family of solutions of (42) consistent with the asymptotic behavior (47) is described by the asymptotic series

$$\bar{F} = \sum_{i=0}^{\infty} c_i |\eta|^{1/2-5i/6}, \tag{49}$$

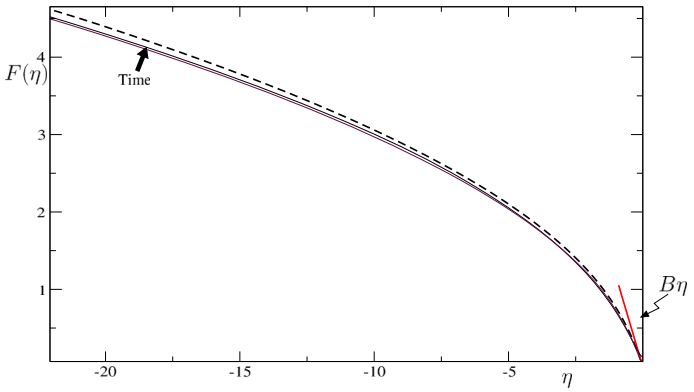

Fig. 10 Solution $F(\eta)$ of (42) with boundary conditions (43) and (47) (*dashed line*); the linear behavior at the origin is also indicated. Results from the numerical simulation of Fig. 6 are shown at times $\log_{10}(t) = 7.8$ and $\log_{10} t = 8.2$, and converge toward the asymptotic solution

where $c_1 = 1$, $c_2 = Q$, and the remaining coefficients c_i are given in (80) in terms of the single parameter Q.

We would like to find a solution to (42) on the interval $(-\infty, 0]$ which is linear near the origin (cf. (43)), and grows like a square root toward infinity, as described by (47). To that end we integrate (42) from near the origin, using the expansion (45), toward $-\infty$. As shown in Appendix 2, the manifold of solutions having the asymptotic behavior (47) has two unstable directions, which carry the solution away from the desired behavior as described by (86). To find the desired solution, we adjust the two free parameters P and B contained in (45), so that the perturbation amplitudes ϵ_1, ϵ_2 remain zero. The values of the constants are

$$B = -1.16978, \qquad P = -0.07164, \tag{50}$$

and the resulting unique solution is shown as the dashed line in Fig. 10. As time goes to infinity, profiles found from a numerical simulation of the full problem agree well with this universal solution.

4.3 Zone III: Static Outer Region

Finally we have to match the right-hand side of the pinch region to the static solution at the end of the bubble, described in Sect. 2.1. In view of (33), the outer limit of the pinch solution behaves like

$$h(x, t) = t^{\alpha_2 - 2\beta_2} A x'^2 = t^{-2/5-\beta_2} A x'^2, \tag{51}$$

which can only match a time-independent outer solution if $\beta_2 = -2/5$. Then according to (44), we find $\alpha_2 = -4/5$. Comparison to (41) shows that the size of the central region is indeed small compared to the typical scale of region I, as required by matching. In both regions, the slope of the interface is asymptotically small: $h_x \ll 1$.

To match (51) to the outer solution, we have to identify the pinch point $x' = 0$ with the maximum of the outer solution, which exists for $\theta_I > \pi/2$ only, see Fig. 3. In that case $R = r(\pi/2)$, and the outer solution has the form

$$h(x') \equiv R - r(x') = \frac{k(R) x'^2}{2} + O(x'^3), \tag{52}$$

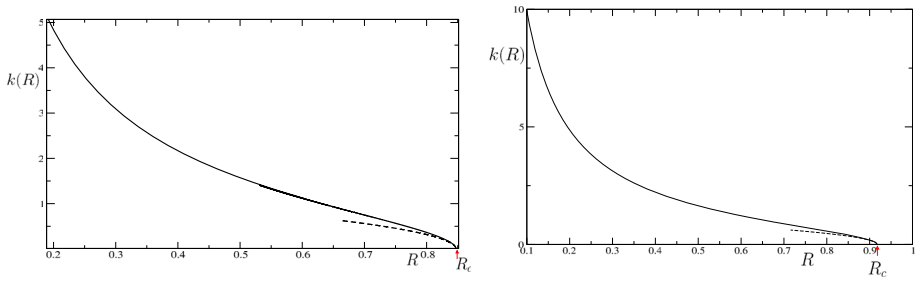

(a) (2D) **(b)** (3D)

Fig. 11 The one-dimensional curvature $k(R)$ as function of the radius. In **a** we show the two-dimensional case (cf. (53)), with the approximation (54) added as the *dashed line*. The corresponding curve in three dimensions, obtained numerically, is shown in **b**, with the approximation (55) shown as the *dashed line*

which matches (51) with $A = k(R)/2 > 0$. Here $k(R) = h_{xx}$ is the (one-dimensional) curvature of the outer solution at $\theta = \pi/2$ (the maximum of $r(\theta)$). The critical case occurs for $\theta_I = \pi/2$, for which $R = R_c$, while matching is not possible for $R > R_c$, for which traveling wave solutions are found.

In two dimensions, using (3) and (4), $k(R)$ is given implicitly by

$$R = \frac{1}{\sqrt{2}} \int_0^{\pi/2} \frac{\cos\psi}{\sqrt{\cos\psi + k^2/2}} d\psi, \tag{53}$$

which is shown on the left of Fig. 11. An approximate form of this curve can be obtained by expanding about the critical value $\theta_I = \pi/2$. According to (22),

$$R = R_c + \frac{K\left(1/\sqrt{2}\right)}{2} \cos\theta_I + O\left(\cos^2\theta_I\right),$$

and thus

$$k(R) = \frac{2\sqrt{R_c - R}}{\sqrt{K\left(1/\sqrt{2}\right)}} \approx 1.468\sqrt{R_c - R} \quad \text{(2D)}. \tag{54}$$

In three dimensions, to obtain $k(R)$, (2) has to be integrated numerically from $\theta = 0$ (the tip) to $\theta = \pi/2$ (the maximum), with $\kappa^{(3D)}$ instead of $\kappa^{(2D)}$. For a given value of the initial condition $\kappa_0 = d\theta/ds$ at $\theta = 0$, one finds the tube radius $R = r(\pi/2)$, and $k = d\theta/ds$ at $\theta = \pi/2$. By varying κ_0, one finds $k(R)$ in parametric form, as shown in Fig. 11 (right). As in two dimensions, the curve ends at $R = R_c$ (R_c being given in (25)), because for $R > R_c$ the profile does not have a maximum. An expansion about $R = R_c$ yields in three dimensions:

$$k(R) = 1.36\sqrt{R_c - R} \quad \text{(3D)}. \tag{55}$$

4.4 The Pinch Region

We can now summarize the properties of the self-similar solution around the pinch point, which has the form

$$h(x,t) = t^{-4/5} H(\xi), \quad \xi = \frac{x'}{t^{-2/5}}. \tag{56}$$

The similarity function $H(\xi)$ is found from (35), where $\hat{H}(\hat{\xi})$ is the universal function shown in Fig. 8. The factors A and B are given by $A = k(R)/2$ and (50), respectively, where $k(R)$ is shown in Fig. 11 (a) and (b). Using the expressions (40) for the scale coefficients, the similarity function becomes

$$H(\xi) = \frac{1.886}{k(R)} \hat{H}\left(\frac{k(R)}{1.786}\xi\right). \tag{57}$$

We now investigate the convergence of the full dynamics to the similarity solution (56), by considering the matching to Zone I and Zone III. In particular, we would like to understand the remarkably slow convergence onto the similarity solution seen in Fig. 8. To that end we estimate the location of the left and right boundary points x_l' and x_r', and their dependence on time. We start with x_l', determined by the matching between Zones I and II.

The flux Q in the pinch region is dominated by the capillary contribution $h^3 h_{xxx}/3$. Since the flux is constant in space, we can calculate it from the asymptotics (34) to find

$$Q \approx \frac{C}{3t^2} = \frac{2\hat{C}B^5\hat{A}}{3\hat{B}^5 k(R) t^2} = \frac{0.687}{k(R)t^2}, \tag{58}$$

which is positive. However, the corresponding flux in Zone I as $\eta \to 0$ is $Q_l = B\eta_l^2/(5t^{9/5})$, which on account of $B < 0$ is negative. Thus there must be a sub-leading correction $\delta(\xi)$ to (56) which makes the flux turn negative as one goes from Zone II to Zone I. Inserting $H(\xi) + \delta(\xi)$ into the *full* similarity Eq. (31) and linearizing in $\delta(\xi)$ one finds to leading order as $t \to \infty$ that

$$\underbrace{t^{-9/5}\left(-\frac{4}{5}H + \frac{2}{5}\xi H_\xi\right)}_{T} + \underbrace{\frac{1}{3}t^{-8/5}\left(H^3\delta_{\xi\xi\xi}\right)_\xi}_{Ca} = 0. \tag{59}$$

Substituting (34) into (59) it follows to leading order that

$$\delta = t^{-1/5}\frac{3}{10B^2}\xi^2 \ln|\xi|, \tag{60}$$

which satisfies $\delta_{\xi\xi\xi} < 0$, and so the flux becomes negative as one passes from Zone II to Zone I. Thus we can define the transition point ξ_l by the condition $|\delta_{\xi\xi\xi}| \approx H_{\xi\xi\xi}$, which results in

$$\xi_l \approx -\left(-\frac{5C}{3B}\right)^{1/2} t^{1/10} \approx -\frac{1.71}{\sqrt{k(R)}} t^{1/10}. \tag{61}$$

In terms of the variable of Zone I, η, this corresponds to

$$\eta_l \approx -\frac{1.71}{\sqrt{k(R)}} t^{-1/10}. \tag{62}$$

Since the scale of the pinch solution is small on the scale of Zone I, the pinch point is located at $\eta = 0$, so η_l goes to zero as expected. The outer limit of the inner (pinch) solution, on the other hand, is $\xi \to -\infty$, which again agrees with (61). The significant point is that in both cases, the convergence toward the expected limit occurs very slowly, which agrees qualitatively with Fig. 8, where it is seen that the point where the full lines start to deviate from the dashed line (the asymptotic solution) moves to the left very slowly.

Now we estimate the location of the transition point x_r' between Zone II and Zone III, for finite time. Zone III is controlled by a static balance between surface tension and gravity, described by $\kappa_x \approx h_{xxx} = 1$. As in the traveling wave solution of Sect. 2, the matching point

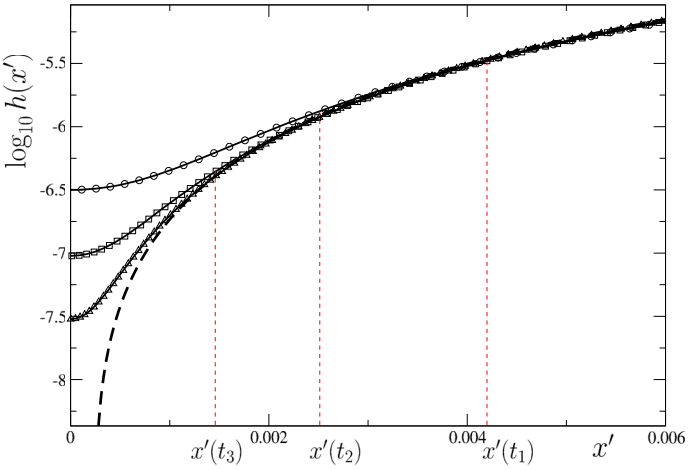

Fig. 12 A close up of the simulation of Fig. 6 near the transition region between Zones II and III, for $t_1 = 2.38 \times 10^9$ (*circles*), $t_2 = 9.66 \times 10^9$ (*squares*) and $t_3 = 4.31 \times 10^{10}$ (*triangles*). In time, curves approach the static outer solution (3),(4) for $R = 0.794 < R_c$ (*dashed line*). The *vertical dashed* (*red*) *lines* indicate x_r' as given by (64) (Color figure online)

is determined by the requirement that $h_{xxx} = 1$, where the left hand side is computed from (56) in the limit $\xi \to \infty$, i.e. (33). This condition yields

$$\frac{2^3 C t^{2/5}}{k^3(R)\xi_m^6} \approx \frac{16.509 t^{2/5}}{k^3(R)\xi_m^6} = 1, \tag{63}$$

which implies

$$x_r' \approx \frac{\sqrt{2}C^{1/6}}{\sqrt{k(R)}} t^{-1/3} \approx \frac{1.596}{\sqrt{k(R)}} t^{-1/3}, \qquad \xi_r \approx \frac{1.596}{\sqrt{k(R)}} t^{1/15}. \tag{64}$$

Once more, in the outer variable (which is the variable x' of Zone III in this case), the transition point goes to zero. The prediction (64) is tested in Fig. 12. The positions x_r', shown for three different times, agree well with the point where the simulation curves start to deviate from the static solution.

4.5 Physical Results

The above calculation completes the description of the solution $R < R_c$ in the limit $t \to \infty$. We now summarize some key results of particular physical significance, explaining in what sense the bubble is "stuck". To ease comparison to experiment, from now on everything will be reported in dimensional form, using the length scale ℓ_c and time scale $\tau = \eta \ell_c / \gamma$.

Using (57), the minimum film thickness reads in dimensional form

$$h_{min} \approx \frac{1.89 \ell_c}{k(R/\ell_c)} \left(\frac{t\gamma}{\eta \ell_c} \right)^{-4/5}, \tag{65}$$

where $k(R/\ell_c)$ is shown in Fig. 11. For $R \lessapprox R_c$ we can use the approximations (54) and (55). If the initial condition is such that $h(x)$ is a film of constant thickness b (apart from the tip region), such as in the simulation shown in Fig. 6, (65) becomes valid only if $h_{min} < b$. This means that the scaling (65) applies for times t with

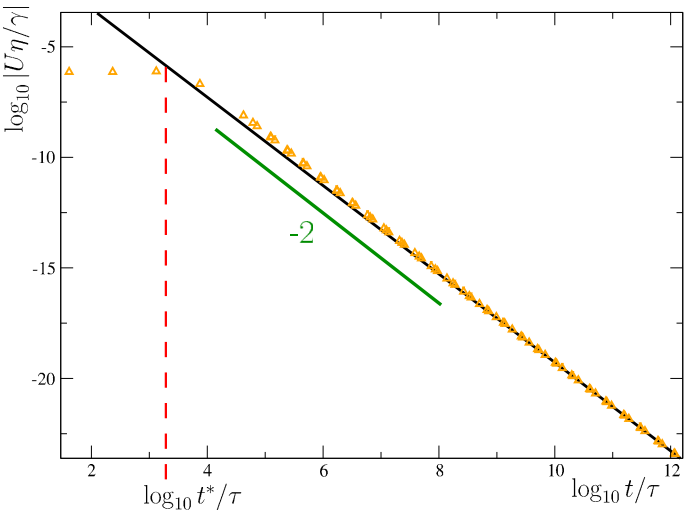

Fig. 13 A comparison between numerical results for the mean speed of a bubble in a 2D tube of radius $R/\ell_c = 0.749$, and the asymptotic behavior $U \propto t^{-2}$. The *solid line* is the scaling (67), *triangles* the numerical results from the run shown in Fig. 6. The *dashed vertical line* marks the time $t^* \approx 2.3 \times 10^3 \tau$ given by (66), beyond which the asymptotic solution applies

$$t > t^* \approx 2.21 \frac{\eta \ell_c}{\gamma} \left(\frac{bk(R/\ell_c)}{\ell_c} \right)^{-5/4}. \tag{66}$$

Apart from the film thickness, the quantity of greatest physical relevance is the speed of the bubble. We estimate the mean motion of the upper part of the bubble, beyond the pinch point, by the total flux across the pinch point, using volume conservation (8) as well as (58). Thus for $R \lessapprox R_c$ one obtains:

$$U(t) \approx -\mathcal{A}^{2D/3D} \frac{\nu \ell_c}{Rg} \frac{t^{-2}}{\sqrt{(R_c - R)/\ell_c}}, \quad \mathcal{A}^{2D} \approx 0.468 \quad \text{and} \quad \mathcal{A}^{3D} \approx 1.01. \tag{67}$$

Note the remarkable fact that asymptotically the flux across the minimum is always positive (owing to the properties of the current equation), so the amount of fluid above the bubble increases. As a result, the bubble is pushed down on average, rather than moving up in the direction of buoyancy.

The asymptotic law (67) agrees very well with numerical simulations, as seen in Fig. 13. One can also see that t^*, as given by (66), is a good predictor of the time beyond which (67) applies. Clearly, the speed goes to zero very quickly, so that the distance traveled in infinite time is finite. Taking as this distance the mean motion of the bubble having started at t^*, we obtain:

$$x_d \approx -\mathcal{A}^{2D/3D} \frac{\eta \ell_c}{\rho R g} \frac{t^{*-1} - t^{-1}}{\sqrt{(R_c - R)/\ell_c}}. \tag{68}$$

Coming back to the surprising observation that according to (67) the bubble appears to move down rather than up, we now show that in an earlier phase of its evolution, the tip of the bubble may in fact be moving up or down, depending on initial condition, at least within the approximate dynamics described by (28). In Fig. 14 we show the velocity U_{tip} as estimated from the flux (27) calculated at the *tip* of the bubble, using two different initial conditions. The first initial condition (corresponding to the dashed line in Fig. 14) is produced in the same way as Fig. 6, obtained by taking a bubble rising under gravity for $R > R_c$, and then

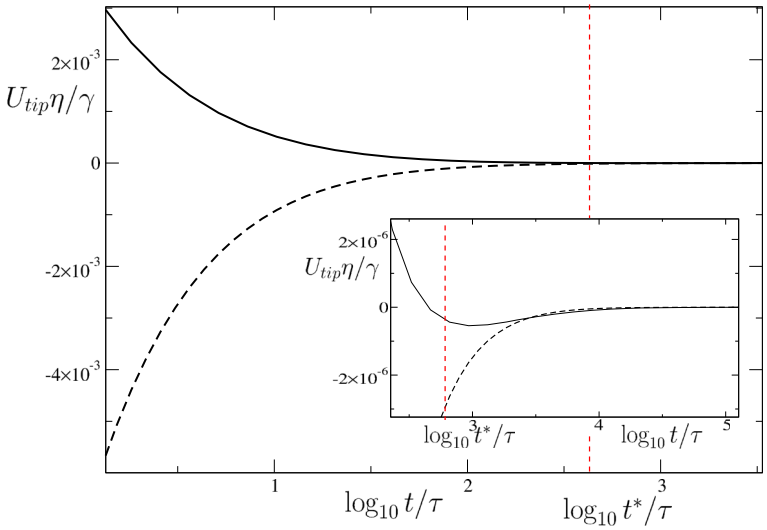

Fig. 14 The velocity U_{tip} at the tip of the bubble as it moves in a tube of radius $R = 0.6/\ell_c$, for two different initial conditions. The initial condition corresponding to the *solid line* is the profile of a bubble being pushed through a tube in the absence of gravity [1], with a film thickness $b/\ell_c = 0.01$. The *dashed line* is produced from a rising bubble as in Fig. 6, but scaled down by a factor of $a = 0.682$. The *inset* is a zoomed-in version of the same plot, showing the change of sign in the *solid line*. The *vertical dashed lines* show the estimated time $t^*/\tau = 670$ for the onset of pinching

rescaling the profile to make it fit into a tube of smaller radius. The second initial condition (corresponding to the full line) is obtained in a more physical way: we start from the profile of a bubble obtained by pushing fluid through the tube (which is the first of the problems considered by Bretherton [1]), which can be achieved simply by *opening* the tube, so that fluid can pass through it.

Firstly, we see that before the beginning of the pinching process at $t = t^*$, typical velocities are much greater than after the profile starts to pinch down. Secondly, the early time dynamics is non-universal, and even the sign of the motion depends entirely on the initial condition. While the dynamics following the second initial condition conforms with our naive expectation that the bubble should move up ($U > 0$), the dynamics following the first initial condition shows the opposite trend: the bubble moves down ($U < 0$). The reason is that in each case, the tip of the bubble relaxes toward its equilibrium shape, which is a semicircle. In the second case, the initial condition is such that its volume is greater than the static outer solution for the top of the bubble. As a result, there is a negative flux to fill this space, corresponding to the bubble moving up. In the case of the first initial condition, the initial bubble shape has a smaller volume than a static bubble, and the bubble moves down. Later in the evolution of the bubble, beyond t^*, the tip velocities for the two initial conditions converge toward one another, as expected for the universal dynamics close to the pinch point.

5 Discussion

The generalized thin film equation (cf. Fig. 15)

$$\frac{\partial h}{\partial t} + \left[h^n h_{xxx}\right]_x = 0, \tag{69}$$

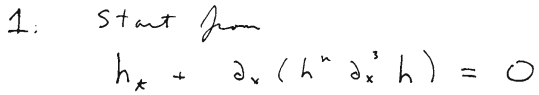

Fig. 15 Equation (69) in the late Leo Kadanoff's handwriting

which has been employed to describe many different physical situations [2–4,7,15,17], plays a central role in our analysis. In the present case of thin film flow over a solid substrate we have $n = 3$; the case $n = 1$ is a model equation for a Hele–Shaw cell [3]. Additional terms may come from gravity, usually subdominant in the pinch region, or from the presence of surface forces. A remarkable property of (69) is that, even for a fixed value of n, it allows for a whole family of different similarity solutions [4], depending on how the equation is driven at the boundaries, or on the initial conditions. As a result, switching between different types of singularities is observed, even after the local dynamics has followed one behavior for many decades [18].

This is in marked contrast to many singularities observed in other systems [8], for example the pinch-off of a fluid jet. Jet pinch-off shows a high degree of universality, in that the similarity exponents and the similarity profile are independent of initial conditions or of the effects of gravity. This difference in behavior can be understood in terms of the physics the respective equations describe. In the case of a three-dimensional jet, surface tension provides an intrinsic mechanism for breakup, as a thinner jet has less surface energy. In the case of a film, no such mechanism exists, if one disregards the effect of "attractive" van der Waals forces [19], which favor thin films, but only come into play for films of about 10 nm thickness and below. For macroscopic films, the energy is independent of the film thickness, and singularities can only be provoked by some external forcing, provided by gravity in the present problem. As a result, it is intuitive that many different types of pinch-off are possible, depending on the details of the forcing provided.

A particular type of singularity revealed in [4] is described by the current Eq. (32), which also lies at the heart of the present analysis. As a further reflection of the intrinsic lack of universality of solutions of (69), the similarity solution in the pinch region has the curious property that the scaling exponents α and β, which describe the shrinking of the film thickness as well as the spatial extent of the pinch region, are not determined by the equation itself. The same holds true of the free constants in front of the asymptotic behaviors (34) and (33).

In [7], Jones and Wilson investigate a solid sphere which falls toward the interface between two viscous fluids. As the top fluid is squeezed out, the thickness of the film of top fluid goes to zero in a region which connects a central region underneath the sphere, and an outer region dominated by surface tension and gravity. A similar solution applies to the merging of two drops under gravity [17]. In both cases, the scaling exponents for the current equation, in the notation of (30), are $\alpha = -1/2$ and $\beta = -1/4$. In [4], infinite time singularities of (69) were analyzed for general n, with the result $\alpha = 1/(1-n)$ and $\beta = 1/(2(1-n))$, consistent with earlier results for $n = 3$.

How can the difference between these earlier results and our result of $\alpha = -4/5$, $\beta = -2/5$ be explained? Firstly, all exponents obey the scaling relation $\alpha = 2\beta$, which comes from the matching to a parabolic outer solution with time-independent curvature on one side of the pinch region. The second exponent is fixed through matching to a "central"region to the other side of the pinch region. Since the scale of the central region is large to that of the pinch region asymptotically, we can expand the profile to linear order about the pinch point x_0.

In the case of (69) considered in [4], the central solution is of the form

$$h(x,t) = t^{\gamma} f(x) \propto t^{\gamma}(x - x_0),$$

and the total flux out of the central region can be written as the time derivative of the total volume, which gives $j \propto t^{\gamma-1}$. This has to be equated with the flux through the pinch region, which is

$$j \propto h^n h_{xxx} \propto t^{(n+1)\alpha-3\beta} \propto t^{(2n-1)\beta},$$

and so $\gamma - 1 = (2n-1)\beta$. Finally matching between the linear regions of the central and pinch regions requires $\gamma = \alpha - \beta$. Combining these scaling relations gives the result $\beta = 1/(2(1-n))$ cited previously.

The crucial difference between previous calculations and the present result is that gravity comes into the balance in the thin film region, which replaces the central region. Since gravity, surface tension, and viscous forces all come in at leading order, exponents in the thin film region are fixed to $\alpha_1 = -3/5$, $\beta_1 = -1/5$ on dimensional grounds. Matching in the linear crossover region, this yields the requirement $-2/5 = \alpha_1 - \beta_1 = \alpha - \beta = \beta$, consistent with (56). Note that the flux, taken in a fixed frame of reference, is now no longer the same between the two similarity solutions.

As we mentioned earlier, on small scales van der Waals interactions come into play. If they are attractive, thin films are energetically favored, leading to finite time thin film pinch-off even above the critical tube radius calculated by Bretherton [20]. As a result, there exists a critical capillary number below which pinching occurs. If on the other hand van der Waals interactions are attractive, pinch-off is inhibited, and the pinch solutions described here are no longer expected to be valid below a thickness of 10 nm.

We expect that in the long-time limit, a new type of traveling-wave solution will be established, the bubble leaving behind a very thin film of uniform thickness. Surprisingly, this thickness is not set simply by the van der Waals length $a = A/(6\pi\gamma)$, where A is the Hamaker constant [19]. Instead, a more detailed calculation, incorporating the van der Waals repulsion into Bretherton's original calculation [21], shows that the speed is now

$$U = \frac{\gamma}{\eta} \frac{a^2}{3R\sqrt{2(R_c - R)\ell_c}}, \tag{70}$$

while the film thickness is

$$b = \frac{a^{2/3}\ell_c^{1/2}}{\sqrt{2}(R_c - R)^{1/6}}. \tag{71}$$

Owing to the quadratic dependence of the speed on a, which is typically one Angstrom, the expected speeds are unfortunately very slow, and observed speeds might well be controlled by other mechanisms, such as roughness.

Finally, we believe the system studied here to be a fertile ground for experiment. The only previous experimental test of the transition between moving and stuck bubbles we are aware of is a qualitative observation of Bretherton himself [1]. As he notes, the verification of (25) might prove difficult, as the transition could be obscured by effects of contamination. By contrast, the pinch phenomenon we discuss in this paper is much more robust, since it is not tied to being close to the transition. We believe this to be an ideal setup to study the pinch-off singularity of a thin film, which to our knowledge has not been reported before.

In order to set up a well-defined initial condition from which the pinching process starts, we propose the following procedure. Prepare a capillary whose radius is below the critical

value, so that the bubble is stuck if the tube is closed. However, by holding the tube vertically and opening the upper or lower end slightly, the bubble will rise at a slow rate, which can be controlled by the size of the opening. From the observed speed of rise U one can calculate the film thickness b using Bretherton's first problem for the motion of a bubble in the absence of gravity [1]

$$b = 0.643R\left(\frac{3\eta U}{\gamma}\right)^{2/3}. \tag{72}$$

Once the opening is closed, the pinch-off process begins, with an initial film thickness given by (72). The minimum thickness should then evolve according to (65).

In conclusion, Leo Kadanoff left a wonderful and lasting legacy with his contributions to the study of singularities. A great many important problems remain, which will be a source of pleasure and fascination for generations of scientists to come.

Acknowledgements We are grateful to Howard Stone for pointing out to us the paradox of the stuck bubble, and for enlightening discussions. Discussions with John Kolinski and Hyoungsoo Kim on the possibility of experiments are also gratefully acknowledged.

Appendix:1 Asymptotics for F as $\eta \to 0$

We would like to find the most general solution of (42) consistent with the linear asymptotics (43). To find the structure of the solution in this limit, we put $F = B\eta + \delta$, where δ is a small correction. Then the leading-order contribution to (42), coming from the first two terms on the left, is linear in η, while $(F^3)_\eta$ is subdominant as $\eta \to 0$. Linearizing the remaining term $(F^3 F_{\eta\eta\eta})_\eta$ in δ, (42) yields:

$$-\frac{2B\eta}{5} + \frac{B^3}{3}\left(\eta^3\delta'''\right)' = 0. \tag{73}$$

Here and in the remainder of this appendix, primes denote the derivative with respect to the argument. Integrating (73) we find the general solution

$$\delta = -\frac{9}{20B^2}\eta^2 + \frac{3\eta^2}{10B^2}\ln(|\eta|) + \delta_1\ln(|\eta|) + \delta_2 + \delta_3\eta + \delta_4\eta^2, \tag{74}$$

where $\delta_1, \ldots, \delta_4$ are constants of integration. The coefficients δ_1 and δ_2 must vanish, since they would dominate (43), contradicting our assumption, while δ_3 can be included in the constant B. Thus the leading behavior of F as $\eta \to 0$ is

$$F = B\eta - \frac{9}{20B^2}\eta^2 + \frac{3\eta^2}{10B^2}\ln(|\eta|) + P\eta^2,$$

with a single free constant P.

The general form of the expansion must contain higher powers of $\ln\eta$ as well, since powers of $\ln\eta$ are generated by the term F^3. A closer inspection shows that the most general expansion which balances the number of free coefficients with the number of equations is

$$F(\eta) = \sum_{j=1}^{\infty}\sum_{i=0}^{\max(j-2,1)} a_{ji}\eta^j\left(\log|\eta|\right)^i, \tag{75}$$

where $a_{10} = B$, $a_{11} = 0$, $a_{20} = P - 9/(20B^2)$ and $a_{21} = 3/(10B^2)$ as shown above. The coefficients a_{ji} are now found recursively as follows. Substituting (75) into (42), at each

order $j \geq 3$ we obtain terms of the form

$$\eta^j (\log|\eta|)^i, \quad i = 0, \ldots, j-1,$$

whose coefficients must equal zero, and which constitute a linear system of equations for $a_{j+1,0}, \ldots, a_{j+1,j-1}$. Starting with $i = j-1$, this system can be solved recursively for $a_{j+1,j-1}$, proceeding down to $i = 0$, which is an equation for $a_{j+1,0}$. Implementing this scheme in MAPLE, we find

$$\begin{aligned} a_{30} &= -\frac{4P}{15B^3} + \frac{19}{75B^5} + \frac{1}{6}, \quad a_{31} = -\frac{2}{25B^5}, \\ a_{40} &= \frac{P^2}{8B^4} - \frac{1}{80B^3} - \frac{131P}{800B^6} + \frac{1507}{32000B^8}, \\ a_{41} &= \frac{3}{8000}\frac{200B^2P - 131}{B^8}, \quad a_{42} = \frac{9}{800B^8}, \quad \ldots. \end{aligned} \tag{76}$$

Appendix: 2 Asymptotics for F as $\eta \to -\infty$

Here we seek a description of solutions of (42) consistent with the asymptotics (47) as $\eta \to -\infty$, so we put

$$F = \sqrt{-\eta} + \delta$$

into (42) and linearize in δ. Contributions coming from surface tension are subdominant at this order, and we obtain to leading order

$$\frac{2}{5}\delta + \frac{6}{5}\eta\delta' = \frac{1}{8\eta^2}, \tag{77}$$

where the right-hand side comes from gravity. This has the general solution

$$\delta = \frac{Q}{(-\eta)^{1/3}} - \frac{1}{16\eta^2}, \tag{78}$$

where Q is a constant of integration.

This suggests a general solution of the form

$$F = \sum_{i=0}^{\infty} c_i |\eta|^{1/2-5i/6}, \tag{79}$$

where all coefficients c_i can be determined uniquely, and contributions from surface tension come in at higher orders. The first few are,

$$c_1 = 1, \quad c_2 = Q, \quad c_3 = -Q^2/6, \quad c_4 = -1/16, \ldots, \tag{80}$$

determined by a single free constant Q.

Next we wish to find all solutions F to (11), which asymptote to $\bar{F}$ as $\eta \to -\infty$, by performing a linear stability analysis around $\bar{F}$, using the ansatz:

$$F = \bar{F} + \delta(\eta). \tag{81}$$

We are interested in all possible $\delta(\eta)$, which grow exponentially as $\eta \to -\infty$. Inserting (81) into (42) and linearizing, we find

$$-\frac{3}{5}\delta + \frac{1}{5}\eta\delta' + \left(\bar{F}^2\delta\bar{F}'''\right)' + \frac{1}{3}\left(\bar{F}^3\delta'''\right)' - (\bar{F}^2\delta)' = 0. \tag{82}$$

Since the coefficients depend on η, we use the WKB ansatz $\delta(\eta) = e^{\lambda(-\eta)^n}$. For $n > 0$, the leading order balance as $\eta \to -\infty$ is

$$-\frac{6}{5}(-\eta)\delta' + \frac{1}{3}(-\eta)^{3/2}\delta'''' \approx 0, \tag{83}$$

which requires $n = 5/6$ for the powers to balance, and we obtain the 4th order eigenvalue equation:

$$\lambda\left[1 + \frac{1}{3}\left(\frac{5}{6}\right)^4\lambda^3\right] = 0. \tag{84}$$

We are interested in roots with positive real part only, since negative roots decay exponentially as we integrate toward $-\infty$ and $\lambda = 0$ corresponds to the solution itself. There are two such eigenvectors with positive roots that solve (84):

$$\lambda_{3,4} = \frac{3}{25}450^{1/3} \pm i\frac{3\sqrt{3}}{25}450^{1/3}, \tag{85}$$

leading to unstable solutions of the form

$$F = \bar{F} + \exp\left(\mathcal{A}\eta^{5/6}\right)\left[\epsilon_1 \sin\left(\sqrt{3}\mathcal{A}\eta^{5/6}\right) + \epsilon_2 \cos\left(\sqrt{3}\mathcal{A}\eta^{5/6}\right)\right], \tag{86}$$

where $\mathcal{A} = \frac{3}{25}450^{1/3}$.

References

1. Bretherton, F.P.: The motion of long bubbles in tubes. J. Fluid Mech. **10**, 166 (1961)
2. Dupont, T.F., Goldstein, R.E., Kadanoff, L.P., Zhou, S.-M.: Finite-time singularity formation in Hele-Shaw systems. Phys. Rev. E **47**, 4182 (1993)
3. Constantin, P., Dupont, T.F., Goldstein, R.E., Kadanoff, L.P., Shelley, M.J., Zhou, S.-M.: Droplet breakup in a model of the Hele-Shaw cell. Phys. Rev. E **47**, 4169 (1993)
4. Bertozzi, A.L., Brenner, M.P., Dupont, T.F., Kadanoff, L.P.: Singularities and similarities in interface flows. In: Sirovich, L. (ed.) Applied Mathematics Series, vol. 100, p. 155. Springer, New York (1994)
5. Boatto, S., Kadanoff, L.P., Olla, P.: Traveling-wave solutions to thin-film equations. Phys. Rev. E **48**, 4423 (1993)
6. Kadanoff, L.P.: Singularities and blowups. Phys. Today **50**(9), 11–12 (1997)
7. Jones, A.F., Wilson, S.D.R.: The film drainage problem in droplet coalescence. J. Fluid Mech. **87**, 263 (1978)
8. Eggers, J., Fontelos, M.A.: Singularities: Formation, Structure, and Propagation. Cambridge University Press, Cambridge (2015)
9. Hinch, E.J.: Perturbation Methods. Cambridge University Press, Cambridge (1991)
10. Wilson, S.D.R., Jones, A.F.: The entry of a falling film into a pool and the air-entrainment problem. J. Fluid Mech. **128**, 219 (1983)
11. Oron, A., Davis, S.H., Bankoff, S.G.: Long-scale evolution of thin liquid films. Rev. Mod. Phys. **69**, 931–980 (1997)
12. Wilson, S.D.R.: The drag-out problem in film coating theory. J. Engg. Math. **16**, 209 (1982)
13. Eggers, J., Stone, H.A.: Characteristic lengths at moving contact lines for a perfectly wetting fluid: the influence of speed on the dynamic contact angle. J. Fluid Mech. **505**, 309–321 (2004)
14. Eggers, J., Dupont, T.F.: Drop formation in a one-dimensional approximation of the Navier-Stokes equation. J. Fluid Mech. **262**, 205 (1994)
15. Duchemin, L., Lister, J.R., Lange, U.: Static shapes of levitated viscous drops. J. Fluid Mech. **533**, 161–170 (2005)
16. Bender, C.M., Orszag, S.A.: Advanced Mathematical Methods for Scientists and Engineers. Mc Graw-Hill, New York (1978)
17. Yiantsios, S.G., Davis, R.H.: Close approach and deformation of two viscous drops due to gravity and van der waals forces. J. Colloid Interf. Sci. **144**, 412–433 (1991)

18. Almgren, R., Bertozzi, A.L., Brenner, M.P.: Stable and unstable singularities in the unforced Hele-Shaw cell. Phys. Fluids **8**, 1356 (1996)
19. Bonn, D., Eggers, J., Indekeu, J., Meunier, J., Rolley, E.: Wetting and spreading. Rev. Mod. Phys. **81**, 739 (2009)
20. Hammoud, N., Trinh, P.H., Howell, P.D., Stone, H.A.: The influence of van der Waals interactions on a bubble moving in a tube (2016). arXiv:1601.00726
21. Eggers, J., Stone, H.A.: unpublished manuscript (2015)